Theoretical scaling of the density limit of lower hybrid current drive caused by parametric decay instability

Kunyu Chen[1,*], *Zhihao* Su[1], *Zikai* Huang[1], *Long* Zeng[1], and *Zhe* Gao[1,**]

[1]Tsinghua University, Department of Engineering Physics, 100084 Beijing, China

Abstract. At high plasma density, the lower hybrid current drive (LHCD) system in tokamaks suffers significant efficiency loss caused by parametric decay instability (PDI) induced in the scrape-off layer (SOL) plasma. There, the lower hybrid waves (LHWs) launched from the antenna deposit a large fraction of their power through PDI, leading to the phenomenon of nonlinear density limit of LHCD. In this paper, we present a self-consistent modelling of the power deposition of LHWs in the SOL plasma by coupling PDI to the propagation of LHWs, the power loss of LHCD is evaluated quantitively, and a theoretical scaling of the nonlinear density limit $n_{\mathrm{PDI}} \propto P_0^{-2/3} L_y^{2/3} T_e \omega_0^2 B_0^{4/3}$ is acquired.

1 Introduction

Lower hybrid current drive (LHCD) [1, 2] is the most efficient method to drive plasma current, control current profile as well as improve energy confinement for tokamaks [3–5]. However, the application of LHCD on future tokamak fusion reactors like ITER faces a serious challenge of the nonlinear density limit, an anomalous efficiency loss at a plasma density lower than the linear limit of wave propagation. The phenomenon has been observed in multiple tokamaks including JET [6, 7], EAST [8, 9], Alcator C-Mod [10, 11], FTU [12] and Tore-Supra [13]. As the plasma density increases, the power of the lower hybrid wave (LHW) launched from the antenna gets transferred to a set of LHWs with lower frequencies, leading to a series of sideband signals in the frequency spectrum of LHWs, and the efficiency of LHCD is significantly decreased when the power transferred to the sideband LHWs becomes comparable to the original LHW [9, 14].

Previous studies attribute the nonlinear density limit of LHCD to the parametric decay instability (PDI) induced in the scrape-off layer (SOL) plasma [8, 14–17]. Here, the LHW launched from the antenna serves as the pump wave, which couples to the low-frequency ion-sound quasi-mode (ISQM) or ion-cyclotron quasi-mode (ICQM) and converts to the sideband LHWs [18]. In these works, the linear growth rate of PDI is used to give a qualitative approximation of the power loss of the pump LHW. By utilizing lithiation, the growth rate of PDI can be decreased; thus, the nonlinear density limit of LHCD is improved [8, 15]. However, when it comes to quantitatively evaluating the PDI efficiency loss and the critical plasma density above which LHCD becomes invalid, the linear growth rate of PDI cannot provide enough information. As a result, in spite of the considerable experimental efforts to achieve effective LHCD at the high-density regime, the validity of LHCD for future tokamak reactors remains uncertain, which makes the idea of achieving steady-state operation on ITER more challenging.

In this paper, we present a theoretical model that enables us to quantitatively evaluate the PDI power loss, and subsequently, the nonlinear density limit of LHCD, at different conditions. The basic concepts of our model are introduced in section 2. The quantitative evaluation of PDI power loss as well as the nonlinear density limit are presented in section 3. Section 4 is a brief discussion about our model and its prediction for the applicability of LHCD in future tokamaks.

2 Modeling of LHCD induced PDI

2.1 PDI coupling and saturation

Aiming at calculating the power loss through PDI, a quantitative model of PDI saturation considering both plasma inhomogeneity and finite pump profile is established [19, 20]. The coupling equations of PDI are

$$\begin{aligned}\left[\epsilon_1(x)+\frac{\partial\epsilon_1}{\partial\omega_1}\cdot i\frac{\partial}{\partial t}-\frac{\partial\epsilon_1}{\partial k_{1x}}\cdot i\frac{\partial}{\partial x}\right]\phi_1 &=\alpha_{L\to1}\phi_0^*\phi_L,\\ \left[\epsilon_L(x)+\frac{\partial\epsilon_L}{\partial\omega_L}\cdot i\frac{\partial}{\partial t}-\frac{\partial\epsilon_L}{\partial k_{Lx}}\cdot i\frac{\partial}{\partial x}\right]\phi_L &=\alpha_{1\to L}\phi_0\phi_1.\end{aligned} \tag{1}$$

Where $j = 0, 1, L$ refers to the pump LHW, the lower sideband LHW, and the low-frequency quasi-mode, ϵ_j refers to the dielectric function of wave j, $\alpha_{i\to j}$ represents the coupling coefficient from daughter wave i to daughter wave j. In Eq.(1), the variation of the dielectric function ϵ_j according to plasma parameters is used to interpret the effect of plasma inhomogeneity, instead of the linear dispersion relations used by Rosenbluth [21, 22], thus our model

*Corresponding author: ky-chen@mail.tsinghua.edu.cn
**Corresponding author: gaozhe@tsinghua.edu.cn

is adapted to the PDI cases where low-frequency quasi-modes are involved.

The solution of Eq.(1) provides the saturation level of sideband LHWs ϕ_{1S} as follows

$$\phi_{1S} = \phi^{(0)} \exp\left(A_{\text{amp}}\right), \tag{2}$$

in which footnote S indicates the steady state of PDI, $\phi^{(0)}$ is the low-frequency fluctuation, and A_{amp} is the amplification factor of PDI. For the cases of LHCD induced PDI, the amplification factor takes the form of [19]

$$A_{\text{amp}} = \int_{r_0}^{r_t} \gamma_0 \mathrm{d}t. \tag{3}$$

Here, the integral is calculated along the trajectory of sideband LHW, with r_0 the departure point and r_t the terminal point. γ_0 is the linear growth rate of PDI that can be written explicitly as

$$\gamma_0 = \mathrm{Re}\left[\frac{-i\alpha_{1\to L}\alpha_{L\to 1}\left|\phi_0^2\right|}{\epsilon_L\left(\partial\epsilon_1/\partial\omega_1\right)} - \nu_1\right], \tag{4}$$

the integration in Eq.(3) is proceeded along the trajectory of the sideband LHW, where $\mathrm{d}t = \mathrm{d}\boldsymbol{l}/\boldsymbol{v}_{1g}$ with $\boldsymbol{v}_{1g}$ the group velocity of sideband LHW and $\mathrm{d}\boldsymbol{l}$ the differentiation of the sideband trajectory. It is noted that the definition of γ_0 in Eq.(4) is different from the growth rate obtained from the nonlinear dispersion relation of PDI in a homogeneous plasma [6, 18]. While solving Eq.(1) to get the amplification factor of PDI, the steady state of the instability (i.e. $\partial_t = 0$) is assumed, and the convective amplification factor A_{amp} represents the spatial growth of the sideband LHW. On the contrary, the spatial variation of daughter waves is neglected and the temporal growth is considered while solving the growth rate of PDI in a homogeneous plasma.

To simplify the integration in Eq.(3), we introduce the pump power flux across the sideband trajectory. When the sideband LHW propagates across the pump LHW region, the pump power flux across the sideband trajectory equals the pump power flux at the antenna mouth P_0 if the pump depletion is neglected. Thus we obtain

$$\begin{aligned} P_0 &= \int W_0 L_y (v_{0gx}\mathrm{d}z - v_{0gz}\mathrm{d}x) \\ &= \int W_0 L_y \left(v_{0gx}v_{1gz} - v_{0gz}v_{1gx}\right)\mathrm{d}t \\ &= W_0 L_y L_z v_{0gx}. \end{aligned} \tag{5}$$

Here, footnotes x, y, z represent the radial, poloidal and toroidal directions, L_y is the poloidal length of the antenna, L_z is the poloidal length of the antenna, and $W_0 = \frac{1}{2}\epsilon_0\left(1+\omega_{\text{pe}}^2/\omega_{\text{ce}}^2\right)k_0^2\left|\phi_0\right|^2$ is the power density of the pump LHW. As we can always shift the sideband trajectory to make it propagate across the pump region and maximize A_{amp}, we may then transform the integration over $\mathrm{d}t$ in Eq.(3) to the integration over $\mathrm{d}P_0$. Thus we get

$$\begin{aligned} A_{\text{amp}} &= \int \frac{\gamma_0 \mathrm{d}P_0}{W_0 L_y\left(v_{0gx}v_{1gz} - v_{0gz}v_{1gx}\right)} \\ &= \left\langle \frac{\gamma_0 L_z}{v_{1gz} - v_{0gz}v_{1gx}/v_{0gx}} \right\rangle. \end{aligned} \tag{6}$$

The brackets in Eq.(6) refer to the average over the sideband trajectory.

2.2 Decay channel analysis

We then turn to the PDI decay channels based on the amplification factor defined in Eq.(6). Previous studies have revealed that the two main sets of PDI decay channels, the ISQM channels where the low-frequency quasi-mode is an ISQM and the ICQM channels where the low-frequency quasi-mode is an ICQM, have distinctive reliances on plasma density. That is, the growth rate of the ICQM channels increases with plasma density, whereas the growth rate of the ISQM channels decreases with plasma density [6, 23]. At a relatively high plasma density ($n_e > 10^{18}/\mathrm{m}^3$), the growth rate of the ICQM channel exceeds that of the ISQM channel and becomes dominant [18]. As a result, the nonlinear density limit of LHCD as well as the significant PDI power loss at high plasma density can be explained only by the ICQM channels. We consider only the ICQM channels while evaluating the nonlinear density limit of LHCD. For further simplification of the amplification factor of ICQM channels, we consider the group velocity of the LHWs neglecting the poloidal magnetic field,

$$\begin{aligned} v_{jg\perp} &= \frac{m_i}{m_e}\cdot\frac{\omega_{\text{LH}}^2}{\omega_j}\cdot\frac{k_{jz}^2 k_{j\perp}}{k_j^4}, \\ \frac{v_{jgz}}{v_{jg\perp}} &= \frac{k_{j\perp}}{k_{jz}} = \sqrt{\frac{m_i}{m_e}\cdot\frac{\omega_{\text{LH}}^2}{\omega_j^2 - \omega_{\text{LH}}^2}}. \end{aligned} \tag{7}$$

where $j = 0, 1$ refers to the pump and sideband LH waves and $\omega_{\text{LH}} = \frac{\omega_{\text{pi}}^2}{1+\omega_{\text{pe}}^2/\omega_{\text{ce}}^2}$ the lower hybrid resonant frequency. As the ICQM channels achieve the largest linear growth rate near the last closed flux surface (LCFS) with plasma density $n_e \sim 10^{19}\mathrm{m}^{-3}$, thus we have $k_{0,1\perp} \gg k_{0,1z}$ and $v_{0,1gz} = c/n_{0,1z}$. Here c is the speed of light and $n_{0,1z} = k_{0,1z}c/\omega_{0,1}$ the toroidal refractive index of LHWs. Utilizing the slab geometry of the pump wave $k_{0y} = 0$ and introducing the scatter angle of PDI $\delta = \angle\boldsymbol{k}_{0\perp}\boldsymbol{k}_{1\perp}$, the amplification factor in Eq.(6) then becomes

$$A_{\text{amp}} = \left\langle n_{1z}\gamma_0 \cdot \frac{L_z}{c\left(1-\cos\delta\right)} \right\rangle. \tag{8}$$

Since the growth rate of typical ICQM channels is determined mainly by the $\boldsymbol{E}\times\boldsymbol{B}$ drift coupling terms [18], we find the relationship between γ_0 and δ as $\gamma_0 = \gamma_0|_{\delta=\pi/2}\sin^2\delta$. Therefore, we may use $n_{1z}\,\gamma_0|_{\delta=\pi/2}$ to represent the amplification factor and analyze the behavior of different decay channels.

Figure. 1 shows typical PDI spectrums of both linear growth rate and amplification factor under JET [6] SOL plasma parameters ($n_e = 10^{19}/\mathrm{m}^3, T_i = T_e = 25\mathrm{eV}, B_0 = 2.6\mathrm{T}$) and LHCD settings ($f_0 = 3.7\mathrm{GHz}, n_{0z} = 1.84, P_0 = 2\mathrm{MW}, L_y = 0.348\mathrm{m}, L_z = 0.884\mathrm{m}$). Discrete ICQM decay channels can be found in both spectrums, each of the channels corresponds to a harmonic of ion-cyclotron frequency. The decay channel with $\omega_L \approx \omega_{\text{ci}}$ has the

largest linear growth rate, but the largest amplification factor occurs when $\omega_L > 6\omega_{\rm ci}$, for these decay channels have significantly larger n_{1z}. Since the power loss through each decay channel is determined mainly by the amplification factor, we immediately find that the PDI induced by LHCD mainly transfers the pump LHW power to the sideband LHWs that correspond to the high harmonics of ion-cyclotron frequency and have large n_{1z}. These sideband LHWs are highly damped near the LCFS, thus cannot penetrate into the core plasma and drive plasma current. Consequently, the power transfer from the pump LHW to the sideband LHWs in the SOL region can result in significant LHCD efficiency loss, leading to the nonlinear density limit of LHCD. Similar process can also arise in the SOL region of the high field side (HFS) where the LHW is reflected under the scenarios of weak single pass absorption and strong asymmetry between low field side (LFS) and HFS SOL profiles [14], resulting in the nonlinear density limit of LHCD coupled by the strong sideband LHW signals corresponding to the HFS PDI process instead of the PDI process in the LFS SOL region. In the following contents, we consider mainly the PDI process in the LFS SOL region, for most of the LHCD failures in conventional tokamaks are coupled by the LFS PDI, and the single pass absorption of LHCD will be strong enough on ITER and future fusion reactors.

2.3 The nonlinear density limit of LHCD due to PDI

Using the amplification factor $A_{\rm amp}$, the power loss through PDI takes the form of

$$P_{\rm loss} = \int W^{(0)} \exp\left[2A_{\rm amp}\right] \boldsymbol{v}_{1g} \cdot {\rm d}\boldsymbol{S}. \tag{9}$$

Where $W^{(0)}$ is the power density of plasma fluctuations, and ${\rm d}\boldsymbol{S}$ is the boundary of the pump region. When the amplification factor becomes large enough to make $P_{\rm loss}$ comparable to the pump power flux P_0, the density limit occurs. Recall the power flux of the pump LHW $P_0 = W_0 L_y L_z v_{0gx}$, we immediately find that the $\boldsymbol{v}_{1g} \cdot {\rm d}\boldsymbol{S}$ term has a magnitude similar to the corresponding pump term $L_y L_z v_{0gx}$. Thus, the density limit of LHCD is transformed to a limit of the amplification factor of PDI,

$$A_{\rm amp}^{cr} = \frac{1}{2} \ln\left(\frac{W_0}{W^{(0)}}\right). \tag{10}$$

As the power density of the plasma fluctuations is usually 10 magnitudes lower than that of the pump lower hybrid wave [6, 24], we get an approximation of the critical amplification factor $A_{\rm amp}^{\rm cr} = \frac{1}{2}\ln\left(10^{10}\right) \approx 12$. When the amplification factor of PDI exceeds the critical value 12, the nonlinear density limit of LHCD is observed. Therefore, the nonlinear density limit due to PDI $n_{\rm PDI}$ can be defined through

$$A_{\rm amp}\left(n_{\rm PDI}\right) = 12. \tag{11}$$

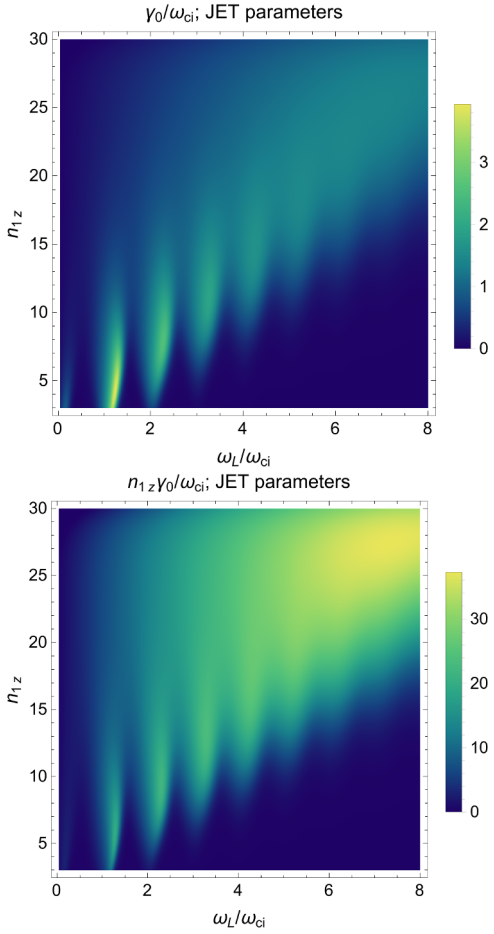

Figure 1. Typical PDI spectrum of linear growth rate and aplification factor, both calculated under the parameters of JET [6], and nondimensionalized by ion-cyclotron frequency

3 Theoretical scaling of the nonlinear density limit

In this section, we scale $A_{\rm amp}$ using both analytical and numerical techniques in order to obtain the theoretical scaling of $n_{\rm PDI}$. The amplification factor defined in Eq.(8) involves three undetermined factors δ, n_{1z} and γ_0. The first two factors interpret the propagation of the sideband LHW, and the third factor describes the growth of PDI along propagation. The scatter angle δ can be determined directly according to the propagation of LHWs. To maximize the amplification factor, we require the sideband LHWs not to propagate into the core plasma in the pump region. Otherwise, the linear growth rate will vanish after the sharp increase of the plasma temperature inside the LCFS [18]. As a result, the scatter angle δ is restricted to a small region near $\frac{\pi}{2}$ unless the toroidal scale of the antenna is small enough to be comparable to the width of the SOL region (i.e. the permissible region of the scatter angle gets larger for Alcator C-Mod and FTU, for their LHW antennas are significantly narrower in the toroidal direction.). For simplicity, we choose $\delta = \frac{\pi}{2}$ in Eq.(8) to obtain

$$A_{\rm amp} = n_{1z}\gamma_0 \frac{L_z}{c}. \tag{12}$$

As the radial scale of the sideband trajectory becomes negligible when $\delta = \frac{\pi}{2}$, the brackets representing the average along the sideband propagation in Eq.(8) are omitted.

We proceed to simplify the $n_{1z}\gamma_0$ term in the amplification factor. The coupling coefficients of PDI have the form of

$$\begin{aligned}\alpha_{1\to L} &= \frac{e\phi_0}{2m_e}\cdot\frac{\chi_{eL}}{k_{Lz}} \\ &\left[-\frac{ik_{0\perp}k_{1\perp}}{\omega_{ce}}\left(\frac{k_{0z}}{\omega_1}-\frac{k_{1z}}{\omega_0}\right)+k_{0z}k_{1z}\left(\frac{k_{0z}}{\omega_1^2}+\frac{k_{1z}}{\omega_0^2}\right)\right], \\ \alpha_{L\to 1} &= \frac{e\phi_0}{2m_e}\cdot\frac{k_L^2}{\omega_1 k_1^2}\cdot(1+\chi_{iL})\left[-\frac{ik_{0\perp}k_{1\perp}}{\omega_{ce}}+\frac{k_{1z}k_{0z}}{\omega_0}\right].\end{aligned} \tag{13}$$

In which $\chi_{iL,eL}$ are the susceptibilities for ICQM with the following form

$$\chi_{sL} = \frac{\omega_{ps}^2}{k_L^2 v_s^2}\left[1+\zeta_s^{(0)}\sum_{n=-\infty}^{+\infty} Z\left(\zeta_s^{(n)}\right) I_n\left(b_s\right) e^{-b_s}\right]. \tag{14}$$

Here $\zeta_s^{(n)} = \frac{\omega_L - n\omega_{cs}}{k_{Lz}v_s}$, ω_{cs}, ω_{ps} and v_s refer to the gyrofrequency, electrostatic oscillation frequency, and thermal velocity of component s. $b_s = k_{L\perp}^2\rho_s^2$ satisfies $b_e \ll 1$ and $b_i \sim 1$.

Substituting Eq.(13) and Eq.(14) into Eq.(4) and Eq.(12), considering the group velocity of LHWs, using the power flux at the antenna P_0 to represent the pump field ϕ_0, and assuming $T_i = T_e$ and $|\omega_0| \approx |\omega_1| \gg |\omega_L|, n_{1z} \approx n_{Lz} \gg n_{0z}$, then Eq.(12) is reduced to the following form.

$$A_{\text{amp}} \propto \omega_{\text{LH}}^3 P_0 L_y^{-1} T_e^{-1}\omega_0^{-2} B_0^{-2}\cdot n_{1z} F\left(\zeta_s^{(n)}, b_i\right). \tag{15}$$

Where function F takes the form of

$$F = \text{Im}\left[\frac{(1+\chi_{iL})\chi_{eL}}{1+\chi_{iL}+\chi_{eL}}\right]\cdot\frac{k_L^2 v_e^2}{\omega_{pe}^2} \tag{16}$$

and the electron-cyclotron term b_e is neglected since $b_e \ll 1$. The toroidal refraction index of the pump LH wave n_{0z} does not appear in Eq.(15) because the experimental setting of n_{0z} among different tokamaks usually satisfies $n_c + 0.5 < n_{0z} < n_c + 1$ where $n_c = \sqrt{1+\omega_{pe}^2/\omega_{ce}^2}$ is the critical refraction rate for the accessibility of LH waves into core plasmas. The group velocity v_{0gx} (and consequently, $|\phi_0|^2$) is insensitive to n_{0z} at such a region, thus the variation of n_{0z} has minimal impact on the PDI process.

Numerical techniques are needed to evaluate the effects of plasma parameters (n_e, T_e, B_0) and LH pump wave parameters (ω_0) on the decay channel n_{1z} as well as the value of the function F. The refraction factor n_{1z} in Eq.(15) can be treated as a function of $\zeta_s^{(n)}$ and b_i. Noticing that $\zeta_s^{(n)} \propto \frac{B_0}{\omega_0 n_{1z}\sqrt{T_e}}$ and $b_i \propto \frac{\omega_{\text{LH}}^2 n_{1z}^2 T_e}{B_0^2}$, we find n_{1z} and F share the same independent variables $\left(\omega_{\text{LH}}, \omega_0, \frac{n_{1z}\sqrt{T_e}}{B_0}\right)$. The effects of the independent variables on both functions are evaluated numerically, thus we find

$$n_{1z} \propto \frac{1}{\sqrt{T_e}}, \quad F \propto \omega_0^{-1}. \tag{17}$$

Substituting Eq.(17) to Eq.(15), we then find the theoretical scaling of A_{amp}.

$$A_{\text{amp}} \propto \omega_{\text{LH}}^3 P_0 L_y^{-1} T_e^{-3/2}\omega_0^{-3} B_0^{-1}. \tag{18}$$

Note that the lower hybrid frequency ω_{LH} satisfies $\omega_{\text{LH}} \propto \sqrt{n_e}$, thus the theoretical scaling of n_{PDI} can be obtained directly through Eq.(18).

$$n_{\text{PDI}} \propto P_0^{-2/3} L_y^{2/3} T_e \omega_0^2 B_0^{4/3}. \tag{19}$$

The theoretical scaling of A_{amp} and n_{PDI} agrees with previous experimental findings among multiple tokamaks. It has been observed on FTU [15] and EAST [25] that utilizing lithiation results in a higher SOL temperature, thus improves the density limit. Increasing the toroidal magnetic field can also suppress PDI and improve the density limit on EAST [9]. The significant improvement of LHCD efficiency in the high-density regime using the 4.6GHz LHW antenna instead of the 2.45GHz antenna on EAST [26, 27] also agrees with the theoretical scaling about pump frequency ω_0 in Eq.(19). Therefore, we may conclude that higher pump frequency, higher SOL temperature, as well as stronger toroidal field can all suppress PDI to improve the density limit of LHCD. Such a scaling also explains the reason that effective LHCD in a plasma density comparable to ITER can be achieved only in strong field devices [15, 16], for these tokamaks have a larger toroidal field and a higher pump LHW frequency.

4 Conclusion and discussion

The nonlinear density limit of LHCD plays an important role in achieving effective non-inductive current drive in future tokamak fusion reactors. In this paper, through combining the power transfer between LHWs by PDI and the linear propagation of LHWs, we modeled the nonlinear power deposition of LHW in the SOL region. When the amplification factor of PDI exceeds a critical level $A_{\text{amp}}^{\text{cr}} = 12$, a considerable fraction of the pump LHW power will be transferred to the sideband LHWs that have large n_{1z} and deposit power near the LCFS through Landau damping, resulting in the anomalous efficiency loss of LHCD. As the amplification factor of PDI increases with plasma density, such a nonlinear mechanism of LHW power deposition can be interpreted by the nonlinear density limit of LHCD.

Through the analytical and numerical evaluation of the amplification factor, we obtained the theoretical scaling of the nonlinear density limit of PDI Eq.(19). The theoretical scaling indicates that the PDI power loss can be suppressed by higher SOL temperature, pump LHW frequency, and toroidal magnetic field, and the dependence of the nonlinear density limit of LHCD on these three parameters agrees with previous experimental findings on multiple tokamaks[6, 7, 9, 14–16, 25, 27]. An approximation of the PDI level based on the theoretical scaling Eq.(18) and Eq.(19) using ITER LHCD system design [28] provides us a crucial insight about the applicability of LHCD for fusion reactors. Note that the SOL density of ITER [29]

is 4 ∼ 5 times larger than that of EAST (the SOL density near the LCFS on EAST is about 10^{19}m^{-3} [17]), whereas the toroidal magnetic field and SOL temperature are both about 2 times higher and the frequency of the LHW source is similar, the amplification factor of PDI on ITER will be lower than that of the EAST 4.6GHz LHCD system according to Eq.(18). As a result, we may conclude that the effect of PDI in the SOL region will be minimal for ITER-like parameters. LHCD remains a promising method of driving plasma current for future tokamaks.

Acknowledgements

This work was supported by NSFC under Grant No. 12335014.

References

[1] N.J. Fisch, A.H. Boozer, Creating an Asymmetric Plasma Resistivity with Waves, Phys. Rev. Lett. **45**, 720 (1980). https://doi.org/10.1103/PhysRevLett.45.720

[2] N.J. Fisch, Theory of current drive in plasmas, Rev. Mod. Phys. **59**, 175 (1987). https://doi.org/10.1103/RevModPhys.59.175

[3] N.C. Hawkes, B.C. Stratton, T. Tala, C.D. Challis, G. Conway, R. DeAngelis, C. Giroud, J. Hobirk, E. Joffrin, P. Lomas et al., Observation of Zero Current Density in the Core of JET Discharges with Lower Hybrid Heating and Current Drive, Phys. Rev. Lett. **87**, 115001 (2001). https://doi.org/10.1103/PhysRevLett.87.115001

[4] Y. Song, X. Zou, X. Gong, A. Becoulet, R. Buttery, P. Bonoli, T. Hoang, R. Maingi, J. Qian, X. Zhong et al., Realization of thousand-second improved confinement plasma with Super I-mode in Tokamak EAST, Science Advances **9**, eabq5273 (2023). https://doi.org/10.1126/sciadv.abq5273

[5] Fujita, T. and Ide, S. and Kamada, Y. and Suzuki, T. and Oikawa, T. and Takeji, S. and Sakamoto, Y. and Koide, Y. and Isayama, A. and Hatae, T. and Kubo, H. and Higashijima, S. and Naito, O. and Shirai, H. and Fukuda, T., Quasisteady High-Confinement Reversed Shear Plasma with Large Bootstrap Current Fraction under Full Noninductive Current Drive Condition in JT-60U, Phys. Rev. Lett. **87**, 085001 (2001). https://doi.org/10.1103/PhysRevLett.87.085001

[6] R. Cesario, A. Cardinali, C. Castaldo, F. Paoletti, W. Fundamenski, S. Hacquin, the JET-EFDA workprogramme contributors, Spectral broadening of lower hybrid waves produced by parametric instability in current drive experiments of tokamak plasmas, Nuclear Fusion **46**, 462 (2006). https://doi.org/10.1088/0029-5515/46/4/007

[7] R Cesario and L Amicucci and C Castaldo and M Kempenaars and S Jachmich and J Mailloux and O Tudisco and A Galli and A Krivska and JET-EFDA contributors, Plasma edge density and lower hybrid current drive in JET (Joint European Torus), Plasma Physics and Controlled Fusion **53**, 085011 (2011). https://doi.org/10.1088/0741-3335/53/8/085011

[8] B. Ding, M. Li, F. Liu, J. Shan, Y. Li, M. Wang, L. Liu, L. Zhao, Y. Yang, Z. Wu et al., Effort of lower hybrid current drive experiments toward to H-mode in EAST, Nuclear Fusion **57**, 022022 (2016). https://doi.org/10.1088/0029-5515/57/2/022022

[9] M. Li, S. Baek, G. Wallace, B. Ding, C. Wu, G. Yan, P. Bonoli, M. Wang, L. Liu, L. Zhao et al., Observation and analysis of lower-hybrid-current-drive density limit in EAST, Nuclear Fusion **62**, 126055 (2022). https://doi.org/10.1088/1741-4326/ac99ed

[10] G.M. Wallace, R.R. Parker, P.T. Bonoli, A.E. Hubbard, J.W. Hughes, B.L. LaBombard, O. Meneghini, A.E. Schmidt, S. Shiraiwa, D.G. Whyte et al., Absorption of lower hybrid waves in the scrape off layer of a diverted tokamak, Physics of Plasmas **17**, 082508 (2010). https://doi.org/10.1063/1.3465662

[11] G. Wallace, A. Hubbard, P. Bonoli, I. Faust, R. Harvey, J. Hughes, B. LaBombard, O. Meneghini, R. Parker, A. Schmidt et al., Lower hybrid current drive at high density in Alcator C-Mod, Nuclear Fusion **51**, 083032 (2011). https://doi.org/10.1088/0029-5515/51/8/083032

[12] V.P. Ridolfini, M. Apicella, G. Calabrò, C. Cianfarani, E. Giovannozzi, L. Panaccione, Lower hybrid current drive efficiency in tokamaks and wave scattering by density fluctuations at the plasma edge, Nuclear Fusion **51**, 113023 (2011). https://doi.org/10.1088/0029-5515/51/11/113023

[13] M. Goniche, V. Basiuk, J. Decker, P. Sharma, G. Antar, G. Berger-By, F. Clairet, L. Delpech, A. Ekedahl, J. Gunn et al., Lower hybrid current drive at high density on Tore Supra, Nuclear Fusion **53**, 033010 (2013). https://doi.org/10.1088/0029-5515/53/3/033010

[14] S. Baek, R. Parker, P. Bonoli, S. Shiraiwa, G. Wallace, B. LaBombard, I. Faust, M. Porkolab, D. Whyte, High density LHRF experiments in Alcator C-Mod and implications for reactor scale devices, Nuclear Fusion **55**, 043009 (2015). https://doi.org/10.1088/0029-5515/55/4/043009

[15] R. Cesario, L. Amicucci, A. Cardinali, C. Castaldo, Current drive at plasma densities required for thermonuclear reactors, Nature Communications **1**, 55 (2010). https://doi.org/10.1088/0029-5515/46/4/007

[16] S.G. Baek, G.M. Wallace, P.T. Bonoli, D. Brunner, I.C. Faust, A.E. Hubbard, J.W. Hughes, B. LaBombard, R.R. Parker, M. Porkolab et al., Observation of Efficient Lower Hybrid Current Drive at High Density in Diverted Plasmas on the Alcator C-Mod Tokamak, Phys. Rev. Lett. **121**, 055001 (2018). https://doi.org/10.1103/PhysRevLett.121.055001

[17] G. Yan, B. Ding, C. Wu, M. Li, S. Baek, F. Napoli, T. Zhou, K. Geng, N. Yan, M. Wang et al., Experimental investigation of PDI bifurcation of lower hybrid waves during electron density ramp-up in EAST, Nuclear Fusion **64**, 086018 (2024).

https://doi.org/10.1088/1741-4326/ad4fa0

[18] A. Zhao, Z. Gao, Parameter study of parametric instabilities during lower hybrid wave injection into tokamaks, Nuclear Fusion **53**, 083015 (2013). https://doi.org/10.1088/0029-5515/53/8/083015

[19] K. Chen, Z. Gao, Saturation of a quasi-mode parametric instability in an inhomogeneous plasma, Nuclear Fusion **65**, 036020 (2025). https://doi.org/10.1088/1741-4326/adb0de

[20] K. Chen, Z. Gao, Analysis of the convective amplification process of a three-wave parametric instability arises from low frequency plasma fluctuation, Plasma Physics and Controlled Fusion **67**, 035026 (2025). https://doi.org/10.1088/1361-6587/adb888

[21] M.N. Rosenbluth, Parametric Instabilities in Inhomogeneous Media, Phys. Rev. Lett. **29**, 565 (1972). https://doi.org/10.1103/PhysRevLett.29.565

[22] M.N. Rosenbluth, R.B. White, C.S. Liu, Temporal Evolution of a Three-Wave Parametric Instability, Phys. Rev. Lett. **31**, 1190 (1973). https://doi.org/10.1103/PhysRevLett.31.1190

[23] Y. Takase, M. Porkolab, J.J. Schuss, R.L. Watterson, C.L. Fiore, R.E. Slusher, C.M. Surko, Observation of parametric instabilities in the lower-hybrid range of frequencies in the high-density tokamak, Physics of Fluids **28**, 983 (1985). https://doi.org/10.1063/1.865070

[24] L. Chen, R. Berger, Spatial depletion of the lower hybrid cone through parametric decay, Nuclear Fusion **17**, 779 (1977). https://doi.org/10.1088/0029-5515/17/4/011

[25] B.J. Ding, M.H. Li, Y.C. Li, M. Wang, J.F. Shan, F.K. Liu, S.L. Wang, W. Wei, H.D. Xu, L.M. Zhao et al., Study of lower hybrid current drive towards long-pulse operation with high performance in EAST, AIP Conference Proceedings **1689** (2015). https://doi.org/10.1088/0029-5515/55/9/093030

[26] M.H. Li, B.J. Ding, F.K. Liu, J.F. Shan, M. Wang, H.D. Xu, L. Liu, H.C. Hu, X.J. Zhang, Y.C. Li et al., Lower hybrid current drive experiments with different launched wave frequencies in the EAST tokamak, Physics of Plasmas **23**, 102512 (2016). https://doi.org/10.1063/1.4965904

[27] M.H. Li, B.J. Ding, F.K. Liu, J.F. Shan, M. Wang, H.D. Xu, R. Cesario, F. Napoli, C. Castaldo, A. Cardinali et al., Experimental investigation on spectral broadening of lower hybrid waves with different frequencies in the EAST long-pulse plasmas, Plasma Physics and Controlled Fusion **61**, 065005 (2019). https://doi.org/10.1088/1361-6587/aaf9da

[28] J.H. Belo, M. Goniche, J. Hillairet, J.P. Bizarro, Optimization of a lower hybrid current drive launcher for ITER, Fusion Engineering and Design **96-97**, 70 (2015). Optimization of a lower 10.1016/j.fusengdes.2015.01.056

[29] S. Carli, R. Pitts, X. Bonnin, F. Subba, R. Zanino, Effect of strike point displacements on the ITER tungsten divertor heat loads, Nuclear Fusion **58**, 126022 (2018). https://doi.org/10.1088/1741-4326/aae43f